Problem Chosen	2026 MCM/ICM Summary Sheet	Team Control Number
B		**2618656**

Feeding More, Fairly: Demand-Corrected Scheduling for Mobile Food Pantries

Summary

Keywords: Food Distribution; Truncated Probability; Spatio-Temporal Symbiosis;scheduling

Contents

1 Introduction

1.1 Background

As the paradigm of human space exploration shifts from short-term mission-based landings toward long-term permanent settlement, Earth's finite resources and fragile ecosystems are compelling us to seek extraterrestrial habitats to facilitate the transition toward a multi-planetary civilization. However, traditional chemical-propulsion rockets face inherent bottlenecks, such as low payload ratios, exorbitant launch costs, and irreversible environmental pollution—which struggle to sustain the massive material transport requirements necessary for large-scale Moon Colony construction. Against this backdrop, the Space Elevator System emerges as a revolutionary interplanetary infrastructure [4]. By synergizing with lunar transfer systems, it is designed to establish a green, efficient, and sustainable logistics chain.

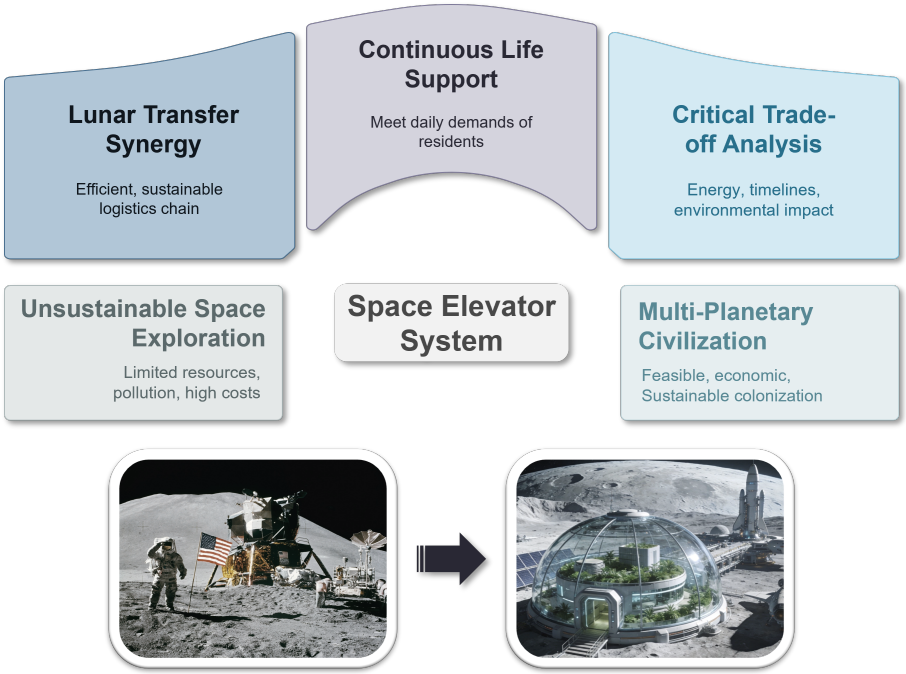

Figure 1: background

The establishment of a large-scale Moon Colony represents both an ultimate test of interplanetary transport capacity and a formidable challenge for the continuous supply of life-support necessities. Within the harsh lunar environment, the daily consumption of 100,000 residents constitutes a persistent logistical demand. When comparing traditional rockets with the emerging Space Elevator System, critical trade-offs must be made regarding energy costs, timelines, launch window constraints, environmental footprints, and the risk-related costs associated with potential system failures. This research is not only central to the feasibility and economic viability of lunar colonization projects but also holds profound significance for the architecture of future interplanetary logistics and the preservation of Earth's ecology.

1.2 Restatement of the Problem

Guided by the constraints provided, we construct a mathematical model to evaluate the optimal cost and schedule for delivering materials to a 100,000-person Moon Colony starting in 2050. The specific tasks are as follows:

- Comparing the logistics and efficiency of three distinct delivery scenarios: utilizing the Space Elevator System's three Galactic Harbours exclusively, relying solely on traditional rocket launches from established sites, or implementing a hybrid transportation strategy .
- Evaluating the robustness of the proposed solutions by analyzing the impact of non-ideal operational conditions, such as mechanical failures or structural instabilities in the elevator and rocket systems .
- Modeling the resource sustainability of the fully operational lunar colony by calculating the additional logistical requirements and costs to ensure a sufficient water supply for one full year .
- Assessing the environmental consequences on Earth's ecosystem under each delivery scenario and optimizing the model to minimize the ecological footprint .
- Providing a strategic recommendation to the Moon Colony Management (MCM) Agency regarding the most viable course of action for building and sustaining the lunar habitat .

1.3 Our Work

2 Model I: Universal Energy-Equivalent and Temporal Coordination Model

2.1 Model Overview

To evaluate Moon Colony logistics, we develop the Universal Energy-Equivalent and Temporal Coordination Model (UETCM). The model adopts Universal Energy-Equivalent (UEE), measured in Joules, as the primary metric to bypass volatile monetary valuations, facilitating a standardized thermodynamic comparison between the momentum transfer of chemical rockets and the gravitational potential gains of the Space Elevator System.

The modeling process begins with establishing a linear mapping between payload mass and energy consumption via the Tsiolkovsky equation and gravitational gradients, integrated with physio-geographical constraints to identify the feasibility gap within the delivery window. To resolve the trade-off between timeline and cost, we introduce the Time Opportunity Cost parameter—derived through a consensus of four independent analytical methodologies—to reformulate the bi-objective optimization into a single-objective framework for identifying the optimal knee point.

Finally, UETCM is extended into a stochastic model incorporating Risk-Adjusted Optimization and Conditional Value-at-Risk (CVaR). Through 10,000 Monte Carlo simulations, we quantify not only the performance impact of perturbations such as tether swaying and system failures but also derive modified strategies with robust safety margins, providing a comprehensive framework that spans from physical mechanisms to resilient strategic decision-making.

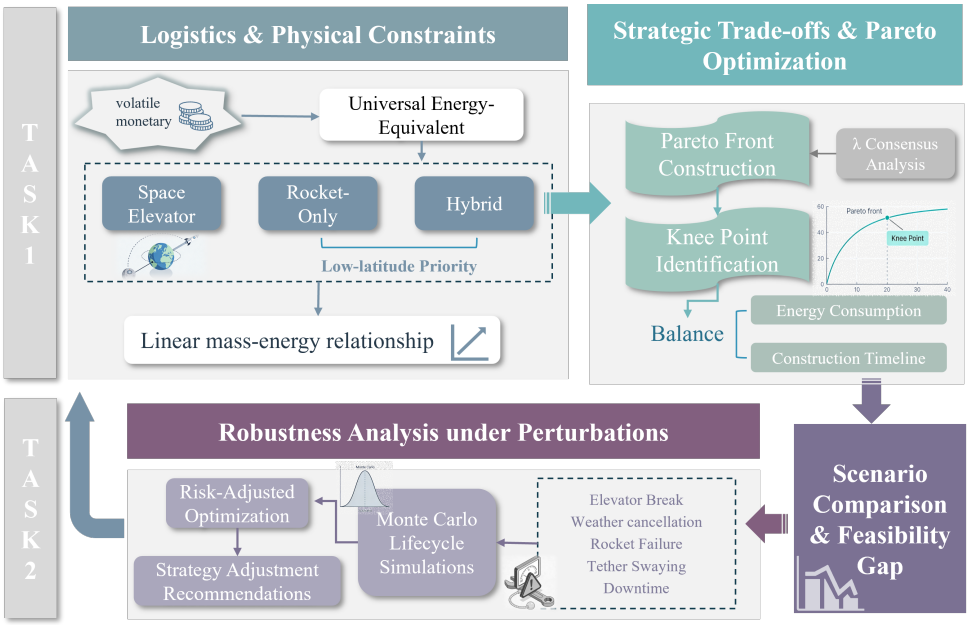

Figure 2: Flow Chart of Model I

2.2 Energy-Equivalent as a Cost Proxy

In traditional economic models, costs are typically measured in monetary terms. However, for an Earth-Moon logistics chain spanning decades, currency is subject to extreme uncertainty driven by inflation and geopolitical shifts. This study posits that in a mature transportation system, energy consumption serves as the optimal proxy for economic cost. To validate this axiom, this section provides multi-dimensional evidence through cost structure analysis, industry data, and statistical correlation.

2.2.1 Cost Convergence Analysis

The operational cost of any transport system, denoted as $Cost(x)$, can be decomposed into hardware amortization, energy consumption, and maintenance:

$$Cost(x) = \frac{C_{hardware}}{x} + C_{energy} + C_{operations} \tag{1}$$

where x represents the reusability or the number of reuse cycles of the transport vehicle. As interplanetary transport technology matures after 2050, x is expected to reach a sufficiently high value, causing the unit manufacturing cost per payload, $C_{hardware}/x$, to be rapidly diluted.

Taking the cost convergence curve of the Boeing 737 as an analogy: as the number of flight cycles increases significantly, the proportion of manufacturing costs drops sharply, while energy costs evolve into the dominant driver of the total cost, consistently stabilizing above 22 percent. In future Earth-Moon logistics, the optimization of energy efficiency will become the sole core path for reducing marginal costs.

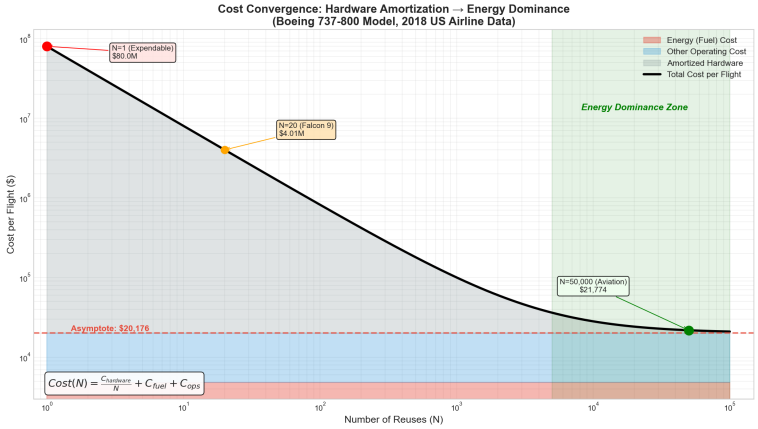

Figure 3: Cost convergence curve demonstrating the transition to energy-dominated cost structures

2.2.2 Empirical Industry Validation

As the most mature large-scale transport system developed by humankind, the aviation industry provides significant reference value. An analysis of U.S. domestic aviation operating data from 1995 to 2018 shows that even amidst volatile oil prices, fuel costs consistently account for 15 to 25 percent of total operating expenses. This confirms that energy is the core cost driver in mature transport systems.

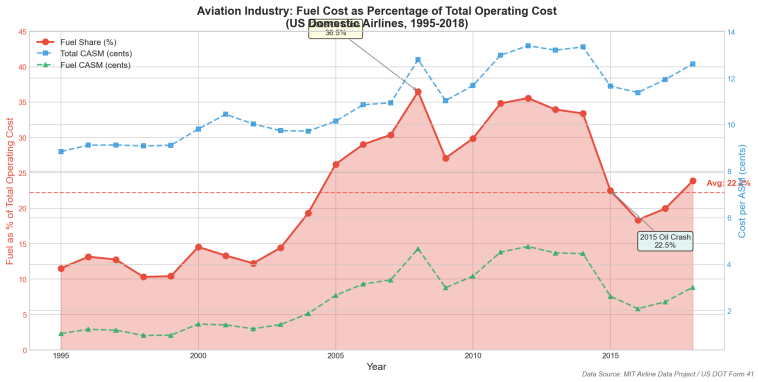

Figure 4: Trend of fuel cost as a percentage of total operating expenses

To further quantify this relationship, we plotted the total cost against energy costs and utilized the Pearson Correlation Coefficient for verification:

$$r = \frac{\sum(C_{total} - \bar{C}_{total})(C_{energy} - \bar{C}_{energy})}{\sqrt{\sum(C_{total} - \bar{C}_{total})^2}\sqrt{\sum(C_{energy} - \bar{C}_{energy})^2}} \tag{2}$$

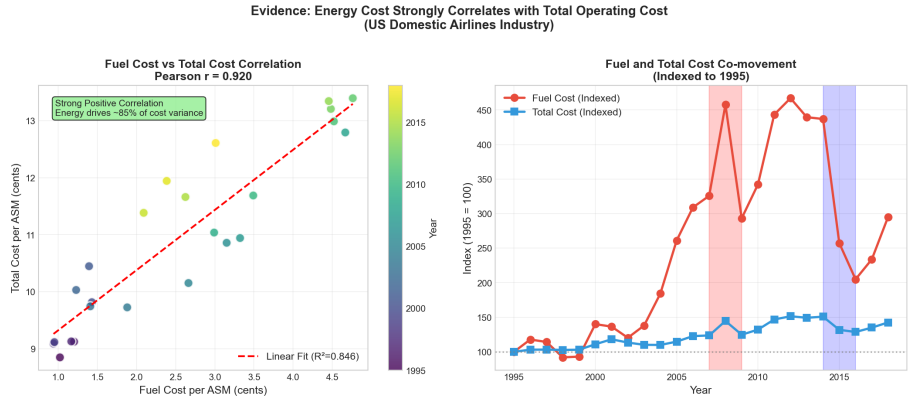

Figure 5: Correlation analysis between total operational costs and energy expenditure

The calculation results reveal a strong linear trend between total cost and energy expenditure, with a correlation coefficient r reaching 0.92. This demonstrates that within a mature transport paradigm, capturing energy consumption is equivalent to capturing the core variance of total economic costs.

In summary, we adopt UEE as the primary metric. Measured in Joules, UEE eliminates inflationary interference and enables a standardized comparison between rockets and elevators. This thermodynamic baseline reflects the physical essence of overcoming gravitational wells. It further aligns with the low-entropy strategic demands of future interplanetary civilizations.

2.3 Ideal Energy Cost Modeling

2.3.1 Rocket Momentum Dynamics

For traditional rocket schemes, the cost depends primarily on the chemical fuel mass required to lift cargo out of Earth's gravitational potential well. We utilize the Tsiolkovsky rocket equation to explore the relationship between fuel consumption and payload.

Step I: Mass ratio constraint analysis

Consider the velocity increment Δv of a rocket neglecting air resistance. We define the mass ratio R as the ratio of initial mass m_0 to final mass m_f:

$$R = \frac{m_0}{m_f} = e^{\Delta V / v_e}$$

where v_e represents the effective exhaust velocity. For a mission such as Trans-Lunar Injection, ΔV is determined by orbital mechanics and is treated as a constant.

Step II: Linear mapping of fuel consumption to payload

A rocket consists of structural mass such as fuel tanks and engines in addition to the payload. We introduce a structural coefficient α, defined as the ratio of structural mass to fuel mass. Through algebraic derivation, the precise ratio of fuel mass m_{fuel} to payload mass m_p is expressed as:

$$m_{fuel} = \underbrace{\frac{R-1}{1-\alpha(R-1)}}_{k} \cdot m_p$$

This formula distills the flight process into a proportional coefficient k. According to the ideal chemical energy release formula:

$$E_{rocket} = \frac{1}{2} m_{fuel} \cdot v_e^2 = \frac{1}{2} k \cdot v_e^2 \cdot m_p$$

This indicates that under traditional rocket modes, energy cost is a linear function of payload mass.

Step III: Total gravitational potential energy transformation

The total energy consumption ΔE is the sum of overcoming Earth's gravity, lunar gravity compensation, and kinetic energy transitions:

$$\Delta E_{total} = m_p \cdot \left[\left(\frac{GM_E}{R_E} - \frac{GM_E}{d_{EM}} \right) - \frac{GM_M}{2r_M} \right]$$

The terms in the formula represent escaping the Earth's surface, the potential energy difference between Earth and Moon positions, and the energy level transition to enter lunar orbit. Consequently, total energy consumption under rocket transport is linearly proportional to the payload mass.

2.3.2 Space Elevator Mechanics

The essential difference between the space elevator and direct rocket flight lies in the primary stage: cargo is first transported along the tether from the Earth Port to the Apex Anchor, then loaded onto a rocket for lunar transit. Since the subsequent rocket segment is covered by the model in the previous section, this section establishes the energy gain model exclusively for the elevator segment.

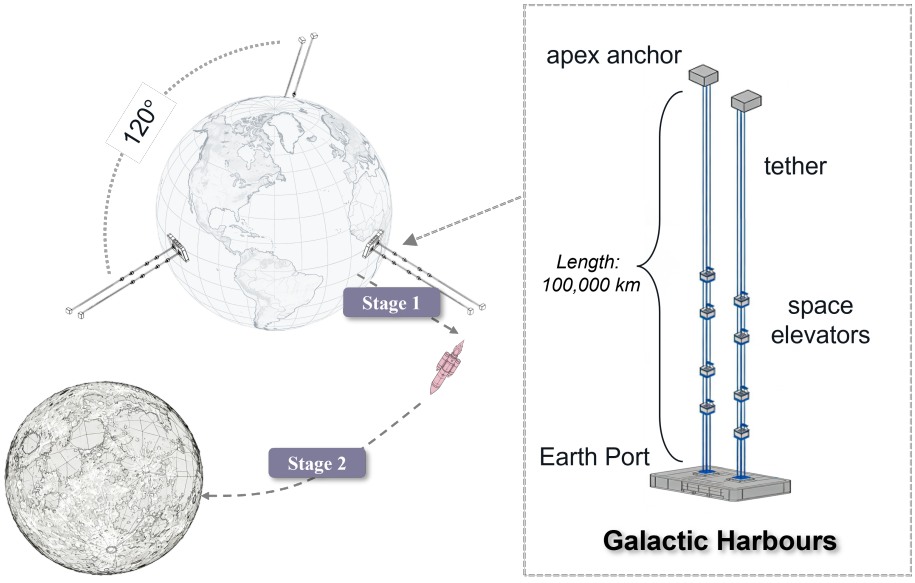

Figure 6: Schematic of the Space Elevator Infrastructure and Earth-Moon Transport Phases

During transport from the Earth Port to the Apex Anchor, the energy change consists of potential energy increase, centripetal kinetic energy gain relative to altitude, and tangential kinetic energy at release:

$$E_{elevator} = m_p \left[\left(\frac{GM_E}{R_E} - \frac{GM_E}{r_0} \right) + \frac{1}{2} \omega^2 r_0^2 \right]$$

where r_0 is the distance from the Apex Anchor to the Earth's center and ω is the Earth's angular velocity. This confirms that elevator transport also maintains a linear relationship between energy consumption and payload.

2.4 Ideal Timeline and Logistic Efficiency Modeling

After resolving the physical energy efficiency, the model determines the construction timeline. The complexity arises from the fact that 100 million metric tons of material cannot be delivered instantaneously; the progress is constrained by the geographical distribution of launch sites, frequency limits, and the inherent capacities of the space elevator and rocket systems.

2.4.1 Transport Progress Formulas

To quantify the construction timeline, the model defines $M_{total} = 10^8$ metric tons as the total demand. Based on the three scenarios provided, the completion time t depends on the annual cumulative capacity C:

- Space elevator only (Scenario a): $t_a = \frac{M_{total}}{C_e}$
- Rockets only (Scenario b): $t_b = \frac{M_{total}}{C_r}$
- Hybrid transport (Scenario c): $t_c = \frac{M_{total}}{\lambda C_e + \mu C_r}$

where C_e is the annual throughput of the space elevator system and C_r is the integrated annual capacity of the rocket system. Shortening the timeline requires increasing annual capacity. By adjusting the hybrid weights λ and μ, we seek a dynamic balance between construction speed and energy cost.

2.4.2 Logistic Efficiency Optimization Under Physio-Geographical Constraints

The primary obstacles to construction progress are geographical constraints and frequency limits, which define the upper bound of C_r.

- **Frequency constraints:**

To estimate the global launch capacity ceiling, we apply a Richards growth model to historical launch data. As shown in Figure 7, the model predicts a theoretical saturation limit of $K = 4298$ annual launches. However, accounting for practical constraints such as maintenance cycles and meteorological windows, we adopt a conservative operational cadence of one launch per day per site (365 annually). This calibrated cap serves as the primary constraint for determining the minimum construction duration.

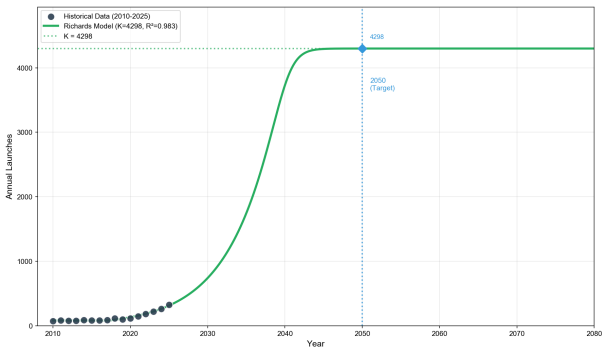

Figure 7: Richards growth model fitting and projected capacity limit K

- **Latitude-based efficiency correction:**

Earth's rotation provides rockets with a tangential initial velocity v_{0i}. The energy gain varies by latitude as follows:

$$v_{0i} = v_{0E} \cdot \cos\theta_i$$

As illustrated in Figure 8, higher latitudes result in lower initial velocities, necessitating more chemical fuel. As latitude increases, the non-linear loss of tangential velocity causes the fuel-to-payload ratio to increase from 31.8 at equatorial sites to 34.0 at high-latitude sites.

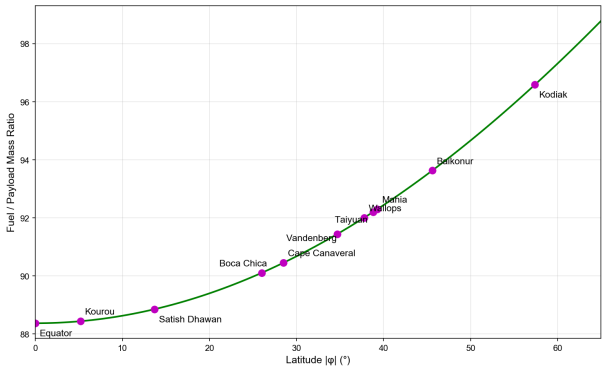

Figure 8: Rotation Velocity and Loss vs Latitude

Consequently, the model implements a low-latitude priority principle: low-latitude sites such as Kourou are prioritized to minimize global energy consumption when the number of launches has not reached the limit. This ensures that for a given timeline, the efficiency of material delivery is maximized.

2.5 Strategic Trade-offs and Multi-criteria Optimization

While the Pareto front effectively visualizes the energy-time trade-off, it does not directly prescribe a specific operating point. To enable principled decision-making, we reformulate the bi-objective optimization problem into a single-objective framework by introducing the time opportunity cost parameter λ.

2.5.1 Single-Objective Reformulation via Time Opportunity Cost

The initial bi-objective mission is reformulated into a single-objective scalar framework to identify a unique operating point:

$$\begin{aligned} &\text{Optimization Target:} \quad \min_x \{E(x), T(x)\} \implies \min_T J(T) = E(T) + \lambda \cdot T \\ &\text{Optimality Condition:} \quad \left.\frac{dE}{dT}\right|_{T=T^*} = -\lambda \end{aligned} \tag{3}$$

Where λ (PJ/year) denotes the *time opportunity cost*—an implicit energy-equivalent penalty incurred for each additional year of construction duration. This parameter accounts for maintenance expenditures and the strategic value of early lunar resource utilization. Under this formulation, the optimal duration T^* is reached when the marginal energy saving rate aligns with the time opportunity cost.

This reformulation offers three key advantages:

- Actionable Decision: It yields a unique optimal point once λ is specified.
- Economic Interpretability: λ quantifies how much energy expenditure the decision-maker is willing to accept to accelerate construction by one year.
- Sensitivity Transparency: The relationship $T^*(\lambda)$ reveals how optimal decisions shift with changing priorities.

2.5.2 Determination of Time Opportunity Cost λ

Rather than relying on subjective judgment, we employ four independent analytical approaches that converge on a consensus value.

Approach 1: Normalized Weight Equilibrium

We reformulate Equation using normalized objectives: $J = \alpha \cdot \tilde{E} + (1-\alpha) \cdot \tilde{T}$. When energy and time are valued equally ($\alpha = 0.5$), the equivalent λ is:

$$\lambda_{eq} = \frac{1-\alpha}{\alpha} \cdot \frac{E_{max} - E_{min}}{T_{max} - T_{min}} = \frac{58547 - 15720}{186.2 - 100.7} \approx 501 \text{ PJ/year} \tag{4}$$

Approach 2: Marginal Efficiency Analysis We define the cumulative efficiency $\eta(T) = \frac{E(T_{min}) - E(T)}{T - T_{min}}$. As shown in Table 1, the 139-year timeline achieves $\eta = 517$ PJ/year, deviating only 2.6% from the global mean (504 PJ/year). This indicates a balanced utilization of the trade-off.

Table 1: Marginal Efficiency at Representative Timelines

Timeline T (years)	Energy E (PJ)	Efficiency η (PJ/year)	Deviation from Mean
110	52,281	674	+33.7%
125	45,102	553	+9.7%
139	**38,750**	**517**	**+2.6%**
160	26,583	539	+6.9%
186	15,720	504	(baseline)

Approach 3: Phase Transition Boundary Sensitivity analysis reveals a critical phase transition at $\lambda_c \approx 480$ PJ/year. Selecting $\lambda = 504$ PJ/year positions the solution just beyond this boundary, representing the minimum departure from cost-optimal behavior while incorporating meaningful time sensitivity.

Approach 4: Feasible Region Centroid

The hybrid feasible region spans $T \in [100.7, 186.2]$ years. Its geometric centroid is $T_{centroid} = 143.5$ years. The 139-year solution deviates only 3% from this centroid.

Convergence and Consensus

Table 2 summarizes the convergence of $\lambda \approx 504$ PJ/year, implying each year of delay carries an opportunity cost equivalent to 3.2% of the minimum energy.

Table 2: Convergence of λ Estimates from Independent Methodologies

Analytical Approach	Implied λ (PJ/year)	Corresponding T^* (years)
Normalized Weight Equilibrium ($\alpha = 0.5$)	501	139
Marginal Efficiency Matching	517	139
Phase Transition Boundary	504	139
Geometric Centroid	$\sim$510	143
Consensus	**504 $\pm$ 10**	**139 $\pm$ 4**

Figure 9: Sensitivity analysis of optimal timeline T^* versus time opportunity cost λ. The consensus value $\lambda = 504$ PJ/year (star marker) yields $T^* = 139$ years.

2.6 Results of Task 1

Through numerical simulation of the 100 million metric ton material transport mission, this study elucidates the intrinsic correlation between construction progress and resource consumption under diverse technical constraints. The findings demonstrate that the optimal transport strategy is not a simple superposition of individual methods but a dynamic equilibrium based on the trade-off between physical energy efficiency and temporal costs.

2.6.1 Quantitative Comparison of Three Transport Scenarios

Based on the model outputs, Table 3 summarizes the core indicators for the three baseline scenarios.

Table 3: Multi-indicator Comparison of Earth-Moon Material Transport Scenarios

Scenario Type	Min Duration (a)	Total Energy (PJ)	Unit Energy (GJ/t)
Elevator-Only (a)	186.2	15,720	157.2
Rocket-Only (b)	219.2	50,609	506.1
Hybrid (c)	100.7	31,537	315.4

Integrating Table 3 and Figure 10, a clear duration-energy trade-off emerges. Rocket-only is limited to 219.2 years with peak energy demand, while elevator-only provides the lowest

energy footprint but requires 186.2 years. The hybrid scenario overcomes these bottlenecks, compressing the timeline to 100.7 years. It is the sole solution for the 100–186 year window and converges to elevator efficiency as duration increases. Ultimately, hybrid transport is indispensable for speed, while the space elevator represents the optimal long-term balance of time and energy.

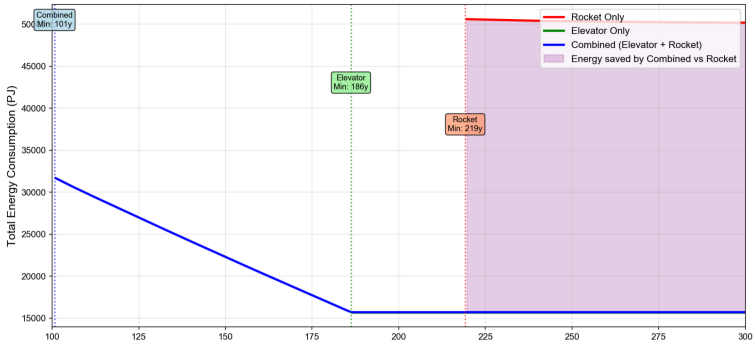

Figure 10: Three Transport Scenarios Feasibility Comparison

2.6.2 Multi-objective Decision-Making via Pareto Front

To optimize the time-energy trade-off, three typical strategies are identified from the Pareto front (100.7–186 years) and detailed in Table 4.

Table 4: Core Metrics of Typical Optimization Strategies for Scenario C

Strategy Type	Duration (a)	Total Energy (PJ)	Elevator Share	Energy Saving
Strategy A (Cost-Prioritized)	186.0	15,720	100.0%	69.0%
Strategy B (Time-Prioritized)	100.7	31,537	54.1%	37.7%
Strategy C (Balanced)	139.0	**38,750**	74.6%	**23.4%**

These strategies represent key Pareto nodes: Strategy A minimizes global energy via full-load elevator operation; Strategy B achieves the shortest timeline through maximum energy input; and Strategy C balances construction efficiency with energy expenditure to provide the basis for capacity allocation.

1. **Marginal Energy Saving**: As shown in Figure 11, the marginal saving curve exhibits a step-wise diminishing trend. Between years 101 and 139, each additional year allocated to the timeline reduces energy demand by approximately 210 PJ. Beyond the 139-year knee point, the marginal conservation rate drops to 185 PJ/a, indicating saturation of energy returns for time invested.

2. **Knee Point Recommendation**: The 139-year duration is recommended as the global optimal point. It extends the minimum timeline by only 38 percent while yielding a 23.4 percent reduction in energy consumption compared to the rocket-only baseline.

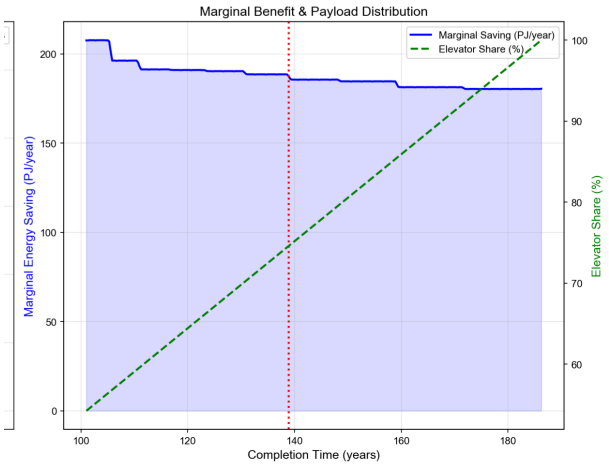

Figure 11: Combined Scenario Pareto Front

2.6.3 Sensitivity Analysis

To assess the robustness of our model, we perform sensitivity analysis on five key parameters. Figure 12 summarizes the results.

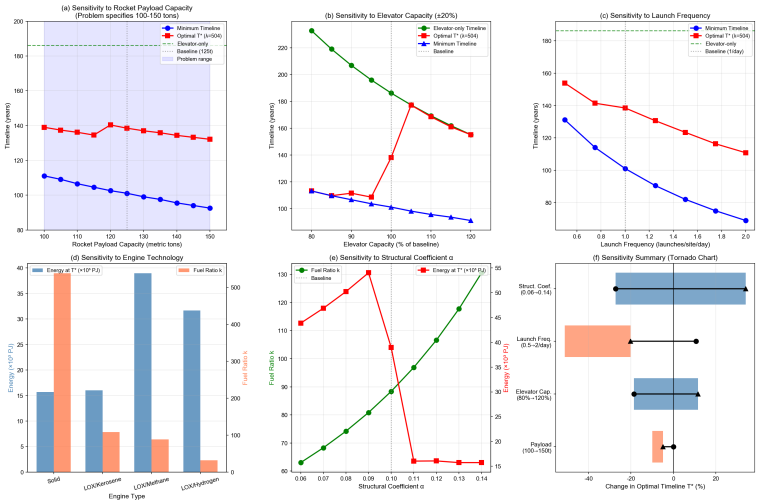

Figure 12: Sensitivity Analysis

- **Rocket Payload Capacity (100–150 tons):** As specified in the problem statement, we analyze the full payload range. Results show that higher capacity reduces minimum timeline from 111 to 93 years, but has limited impact on the optimal hybrid solution at $\lambda = 504$.
- **Elevator Capacity (±20%):** Elevator capacity emerges as the most sensitive parameter. A 20% reduction extends the elevator-only timeline from 186 to 233 years, fundamentally altering the hybrid strategy's feasible region.
- **Launch Frequency:** Doubling launch frequency from 1 to 2 per day reduces minimum timeline from 101 to 69 years, enabling more aggressive time-optimized strategies.

- **Engine Technology:** Engine Isp primarily affects energy consumption rather than timeline. LOX/Hydrogen (Isp=450s) reduces fuel ratio by 64% compared to LOX/Methane, but practical considerations favor the latter.

Table 5: Sensitivity Analysis Summary

Parameter	Range	Impact on T^*	Impact on E^*
Payload Capacity	100–150 t	Low	Low
Elevator Capacity	±20%	High	Medium
Launch Frequency	0.5–2/day	Very High	Low
Engine Isp	350–450 s	Low	High
Structural Coef.	0.06–0.14	Medium	High

2.7 Risk-Adjusted Strategy Optimization Under Non-Perfect Conditions

Task 2 asks a fundamentally different question from Task 1: not merely how much performance degrades, but how our recommended strategy should change in response to system uncertainties. We achieve this through a three-stage methodology: quantifying perturbation impacts, identifying risk-adjusted decision boundaries, and finally deriving modified optimal strategies with robust safety margins.

2.7.1 Quantification of Stochastic Perturbations

Given the unprecedented nature of the Space Elevator System, we acknowledge significant epistemic uncertainty in failure parameters. We adopt a conservative approach by establishing parameter ranges rather than point estimates:

Table 6: Perturbation Parameter Ranges and Sources

Parameter	**Baseline**	**Range**	**Basis**
Tether swaying ($\Delta\theta$)	0°	$[-0.5^\circ, 0.5^\circ]$	Coriolis-induced oscillations during release
Rocket failure rate	0.75%	[0.3%, 1.5%]	Falcon 9 historical [2] + technology maturation
Elevator breaks/year	2	[1, 4]	IAA Space Elevator Assessment [5]
Downtime per break	14 days	[7, 30] days	Scaled from offshore platform repairs
Weather cancellation	10%	[5%, 20%]	Site-specific meteorological data

2.7.2 Risk-Adjusted Optimization Framework

Under uncertainty, the deterministic objective function must be extended to incorporate risk preferences. We reformulate the optimization as:

$$\min_{T} \quad J_{robust}(T) = \mathbb{E}[E(T)] + \lambda \cdot \mathbb{E}[T] + \gamma \cdot \text{CVaR}_\alpha(T) \tag{5}$$

where $\text{CVaR}_\alpha(T)$ denotes the Conditional Value-at-Risk at confidence level α (typically 95%), representing the expected completion time in the worst $1-\alpha$ scenarios. The risk aversion coefficient γ (PJ/year) quantifies the MCM Agency's willingness to pay for reduced schedule uncertainty.

2.7.3 Monte Carlo Lifecycle Simulation

Due to the highly non-linear interactions between these stochastic variables, we utilized a Monte Carlo algorithm to execute 10,000 simulations of the construction cycle.

- **Simulation Logic**: For each simulated day, the algorithm samples the system state (Normal/Failure/Weather). In the event of interference, payload distribution is adjusted and incomplete tasks are rescheduled.
- **Distribution Analysis**: As shown in Figure 13, the results exhibit a significant right-skewed distribution. This implies that real-world timelines are prone to a long tail of cumulative delays—the probability of massive delays is low but the impact is profound, serving as a critical basis for risk assessment.

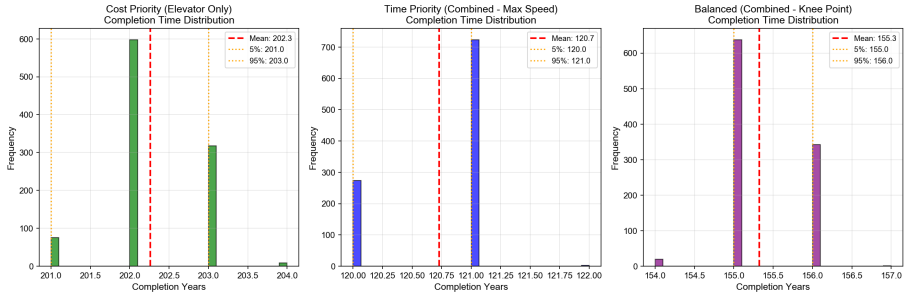

Figure 13: Completion Time Distribution Under Perturbations

2.8 Results of Task 2

Idealized models define the theoretical limits, but stochastic variables such as tether swaying, equipment failure, and weather interference cause performance to deviate. We evaluate system performance under disturbance based on 1,000 Monte Carlo iterations.

2.8.1 Quantitative Comparison of Performance Loss

Table 7 compares the deterministic solutions with stochastic means, quantifying the costs of system perturbations.

Table 7: Comparison of Core Metrics Under Perfect and Non-Perfect Conditions

Strategy Type	Dimension	Perfect Condition	Non-Perfect (Mean $\pm$ Std)	Change Rate
Strategy A	Time (a)	186.2	202.3 ± 0.6	+8.6%
	Energy (PJ)	15,720	$15{,}738 \pm 0$	+0.1%
Strategy B	Time (a)	100.7	120.7 ± 0.4	+19.9%
	Energy (PJ)	31,537	$30{,}217 \pm 30$	-4.2%
Strategy C	Time (a)	139.0	155.3 ± 0.5	+11.7%
	Energy (PJ)	**38,750**	$\mathbf{38{,}285 \pm 45}$	-1.2%

2.8.2 Strategy Adjustment Under Uncertainty

The Monte Carlo results reveal that perturbations do not merely shift performance metrics—they fundamentally alter the risk-return profile of each strategy:

(1) Optimal Timeline Adjustment

Under perfect conditions, the balanced strategy yields $T^* = 139$ years. However, incorporating the 95th percentile delay, the effective planning horizon becomes:

$$T^*_{adjusted} = T^* + \Delta T_{buffer} = 139 + 16.3 \times 1.15 \approx 158 \text{ years} \tag{6}$$

where the 15% margin accounts for tail-risk scenarios. Recommendation: MCM Agency should plan for a 155-160 year timeline to achieve 95% confidence in completion.

(2) Hybrid Ratio Adjustment

Given that elevator breaks dominate schedule risk (correlation = 0.836), the optimal elevator share should be reduced to enhance redundancy:

$$\text{Elevator share}_{adjusted} = 74.6\% - \Delta_{redundancy} \approx 65\% - 70\% \tag{7}$$

This increases rocket utilization as a "backup channel," accepting a 5-8% energy penalty in exchange for improved schedule resilience.

(3) Strategic Reserve Capacity

We recommend maintaining a 10% reserve margin in annual transport capacity:

$$C_{reserve} = 0.1 \times (\lambda C_e + \mu C_r) \tag{8}$$

This reserve can absorb localized disruptions without triggering cascading delays.

2.8.3 Evolution of Key Indicators

Stochastic disturbances transform deterministic values into probability distributions, but the strategic ranking remains robust.

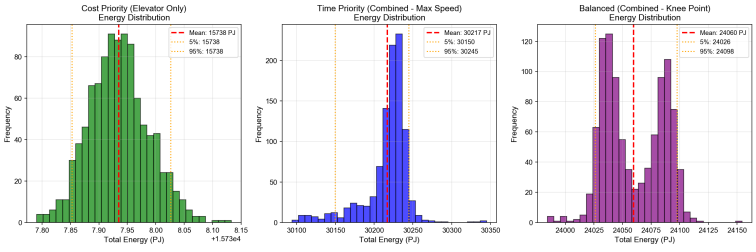

Figure 14: Energy Distribution

- **Energy Stability**: As illustrated in Figure 14, energy consumption follows a narrow-peak normal distribution with a standard deviation of less than 0.2%. This confirms that tether swaying does not cause energy collapse. The slight mean shift in Strategies B and C is due to payload loss from rocket failures offsetting energy increments from swaying.
- **Temporal Right-Skewed Characteristics**: Box plots in Figure 15 reveal that median durations delay by 8.6% to 19.9%. However, the duration intervals for each strategy remain strictly separated, ensuring that the fundamental decision logic—Strategy A for cost and Strategy B for speed—holds true even under perturbation.

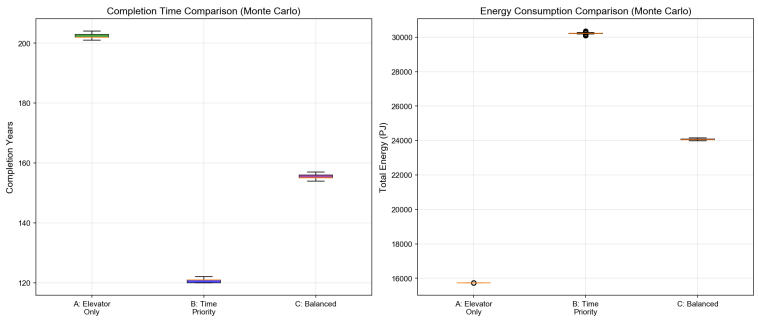

Figure 15: Completion Time and Energy Consumption Comparison

3 Model II:Life-Support Logistics and Stochastic Water Balance Model

3.1 Model Overview

As the Moon Colony transitions from the construction phase to the operational phase, the logistical focus shifts from structural materials to life-support supplies. We develop the Life-Support Logistics and Stochastic Water Balance Model (LSL-SWBM) to quantify the water security boundaries of the settlement during its first year of operation. This model accounts for multi-level demand functions based on psychological comfort and incorporates a normal approximation to address stochastic medical emergency needs. By mapping these water requirements onto the transport framework established in Model I, we evaluate the additional pressure exerted by different comfort factors on the Earth-Moon logistics chain.

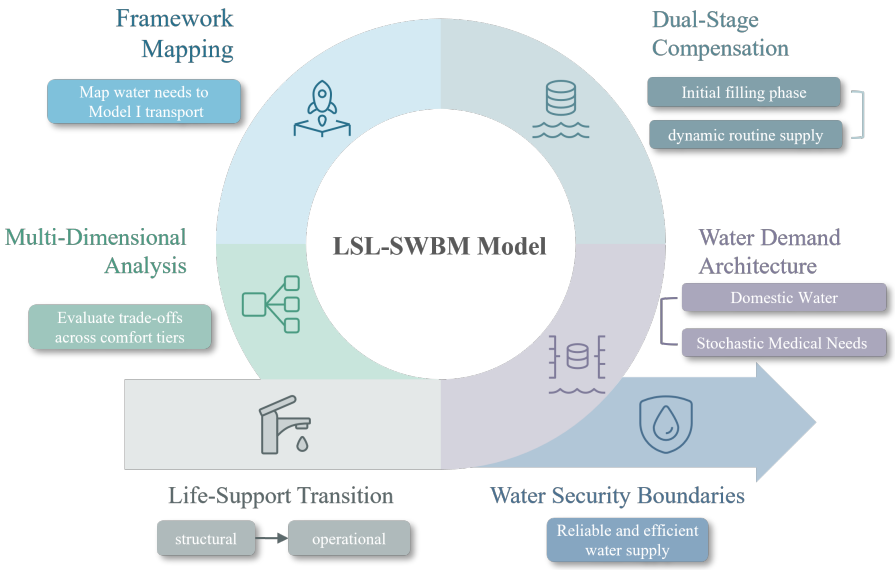

Figure 16: Flow Chart of Model II

3.2 Water Demand Architecture

In an isolated lunar ecosystem, water consumption is primarily sustained by a recycling system [3]. However, logistical replenishment must compensate for system losses and sudden

medical surges. This model assumes that lunar water use is restricted to domestic and medical emergency purposes, excluding industrial use, to define the core demand framework.

3.2.1 Domestic Water Evolution

Within the colony, domestic water consists of survival and hygiene components. The daily demand is formulated as:

$$W_r = N \times (w_s + 0.4\alpha) \tag{9}$$

where N is the population, w_s represents the survival baseline, and α is the comfort factor. The following table summarizes the water standards across different demand tiers [1][6]:

Table 8: Water Demand Standards Across Different Comfort Tiers

Demand Tier	α **Value**	**Daily Use per Capita**	**Description**
Survival Standard	1	2.9 L	Minimum survival threshold
Comfort Standard	50	22.5 L	Moderate domestic comfort
Luxury Standard	250	102.5 L	Equivalent to Earth-like usage

3.2.2 Stochastic Assessment of Medical Emergency Water

Given the large population , the daily number of patients X (assuming a daily incidence rate $p = 2\%$) follows a binomial distribution, which is accurately approximated by a normal distribution $X \sim N(Np, Np(1-p))$. To ensure medical safety under extreme conditions, the model adopts the peak demand at a 99% confidence level as the daily reserve target:

$$W_{medical} = (E(X) + Z_{0.99} \cdot \sigma) \times 5 \text{ kg} \tag{10}$$

This indicator remains stable across different domestic comfort scenarios, ensuring the robustness of the medical support system.

3.3 Logistics Strategy: Initial Filling and Dynamic Compensation

Unlike construction materials, water is highly recyclable. Given the maturity of water recycling technology, the cumulative rate of daily demand after the initial transport is relatively slow. Since a daily delivery schedule would be prohibitively expensive, we adopt a monthly supply mode based on a dual-stage replenishment logic.

3.3.1 Initial Month Filling

During the first month, recycled water from the previous month is unavailable. Thus, the initial supply must satisfy two criteria: providing domestic water for 30 days and maximizing medical reserves for potential surges. The initial transport volume is defined as:

$$W_{initial} = (W_r + W_{mi}) \cdot T \tag{11}$$

where $T = 30$ days and W_{mi} is the daily emergency medical supply at a 99% confidence level. This strategy establishes the system's circulating base while creating a 30-day emergency buffer.

3.3.2 Monthly Routine Compensation

In subsequent months, domestic demand is met through a combination of Earth-based replenishment and water recycling. Simultaneously, medical reserves need only cover the mean incidence rate due to the confidence buffer established initially. With a recycling efficiency η (set at 0.9), the routine monthly supply model is:

$$W_{routine} = (W_r(1-\eta) + W_m) \cdot T \tag{12}$$

This model precisely offsets recycling losses and daily medical consumption to maintain a dynamic water balance.

3.4 Results and Multi-dimensional Analysis for Task 3

Based on the model simulation results, we perform a quantitative decomposition of the water replenishment mission across both temporal and energetic dimensions.

3.4.1 Comparison of Demand Scales across Scenarios

Minute variations in the comfort factor α trigger significant shifts in logistical scale. The water demand metrics for the three simulated scenarios are summarized in Table 9.

Table 9: Water Demand Metrics under Different Comfort Scenarios

Demand Tier	α	**Water Inventory** (t)	**Daily Rep.** (t)	**Initial Trans.** (t)	**Annual Total** (t)
Survival Standard	1	290	29.1	1,163	10,622
Comfort Standard	50	2,250	225.1	9,003	82,162
Luxury Standard	250	10,250	1,025.1	41,003	374,162

Table 9 clearly illustrates the multiplier effect of psychological comfort on logistical scale: as the standard shifts from Survival ($\alpha = 1$) to Luxury ($\alpha = 250$), the annual replenishment requirement surges from approximately 10,000 to over 370,000 metric tons— a jump of more than 35-fold.

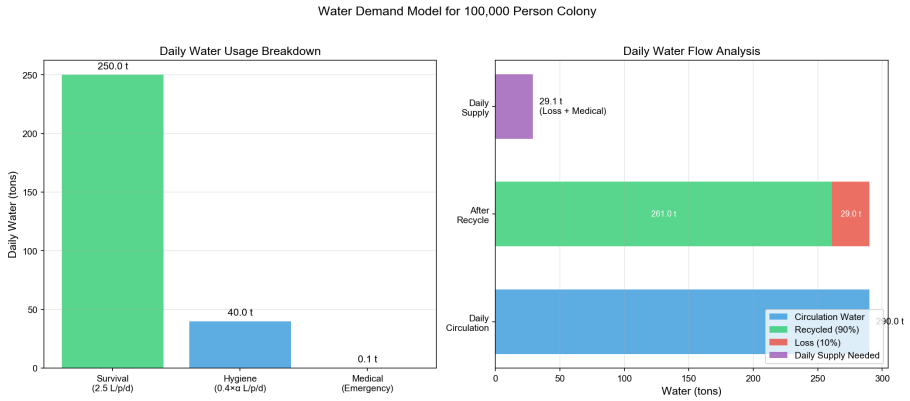

Figure 17: Decomposition of water demand components for the Survival Scenario ($\alpha = 1$)

Taking the Survival Scenario ($\alpha = 1$) as an example, Figure 17 delineates the composition of water demand. Supported by a high-efficiency recycling system, the daily volume required from Earth accounts for only a small fraction of the total demand, underscoring the critical value of closed-loop life-support systems.

3.4.2 Trade-off Analysis of Transport Schemes

To satisfy the aforementioned water requirements, we mapped the demand indicators onto the transport framework of Model I to evaluate four distinct transport schemes. The definitions and baseline capacity comparisons for these schemes are detailed as follows:

Table 10: Definition and Baseline Capacity of the Four Transport Schemes

Scheme	Description	Daily Capacity (t/d)	Specific Energy (GJ/t)
1	Space Elevator Only (3 units)	1,471	157.2
2	Rocket-Only (10 sites)	1,250	506.1
3	Hybrid (Elevator + 10 sites)	2,721	317.5
4	Hybrid (Elevator + Low-lat.)	1,971	243.5

The data indicates that Scheme 3 offers the highest aggregate daily throughput, whereas Scheme 1 provides superior energy efficiency. Although rockets offer viable capacity, their energy cost is approximately 3.2 times that of the space elevator. By integrating the demand tiers with these schemes, we derive the following performance analysis:

(1) Survival Scenario ($\alpha = 1$)

Table 11: Transport Performance Metrics for the $\alpha = 1$ Scenario

Scheme	Initial Days	Initial Energy (TJ)	Monthly Days	Annual Energy (PJ)
Scheme 1	0.79	182.8	0.59	1.67
Scheme 2	0.93	588.6	0.69	5.38
Scheme 3	0.43	369.2	0.32	3.37
Scheme 4	0.59	283.1	0.44	2.59

As shown in Table 11 and Figure 18, all schemes can complete monthly replenishment within one day under low-demand conditions. Scheme 1 demonstrates an absolute advantage in efficiency , while Scheme 3 minimizes delivery time . This suggests that water transport poses minimal pressure on the logistics chain in survival mode.

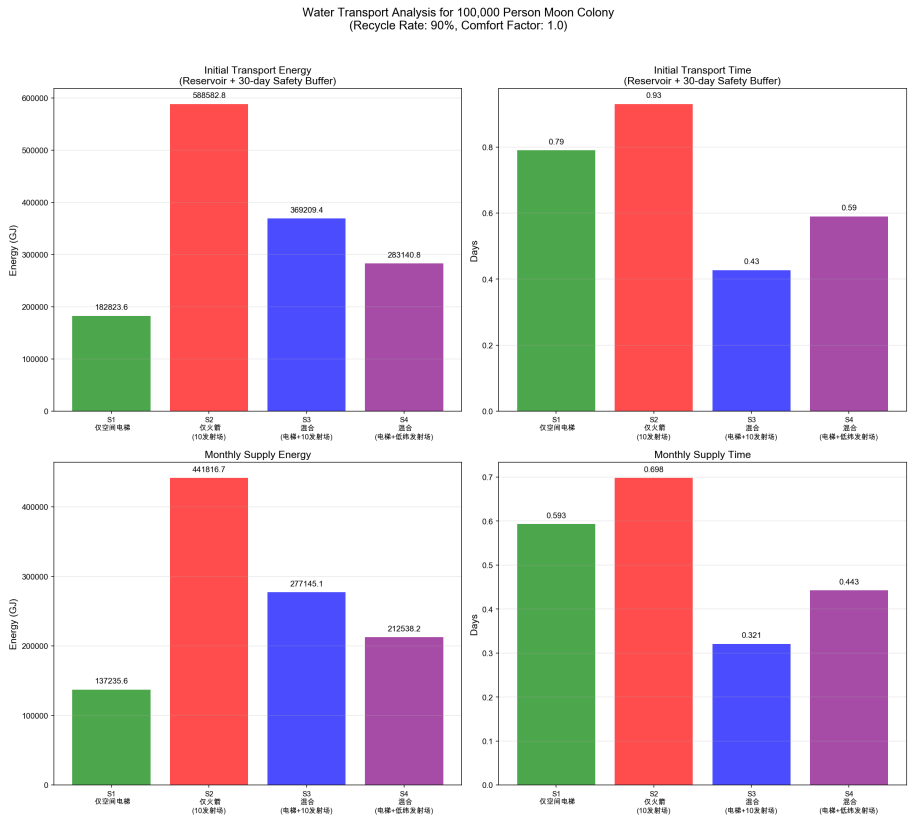

Figure 18: Comparison of transport duration and energy for the $\alpha = 1$ scenario

(2) Comfort Scenario ($\alpha = 50$)

As demand increases eightfold, logistical pressure rises significantly. Under Table 12, Scheme 1 can still complete initial filling within 6.12 days, though annual energy consumption increases to 12.92 PJ. Scheme 4 provides a well-balanced equilibrium between timeline and energy.

Table 12: Transport Performance Metrics for the $\alpha = 50$ Scenario

Scheme	Initial Days	Initial Energy (TJ)	Monthly Days	Annual Energy (PJ)
Scheme 1	6.12	1,415.3	4.59	12.92
Scheme 2	7.20	4,556.3	5.40	41.58
Scheme 3	3.31	2,858.1	2.48	26.08
Scheme 4	4.57	2,191.9	3.43	20.00

(3) Luxury Scenario ($\alpha = 250$)

In this extreme scenario, water logistics becomes a major logistical burden. Table 13 reveals that relying solely on Scheme 1 requires nearly a month for initial filling, with annual energy consumption reaching 58.82 PJ.

Table 13: Transport Performance Metrics for the $\alpha = 250$ Scenario

Scheme	Initial Days	Initial Energy (TJ)	Monthly Days	Annual Energy (PJ)
Scheme 1	27.87	6,445.7	20.90	58.82
Scheme 2	32.80	20,751.2	24.60	189.36
Scheme 3	15.07	13,016.9	11.30	118.78
Scheme 4	20.80	9,982.5	15.60	91.09

Remarkably, even under the Luxury Standard, the annual energy for water transport accounts for only 0.37% of the total construction energy (15,720 PJ) calculated in Model I. This validates that the primary bottleneck is not energy availability, but rather transport capacity allocation.

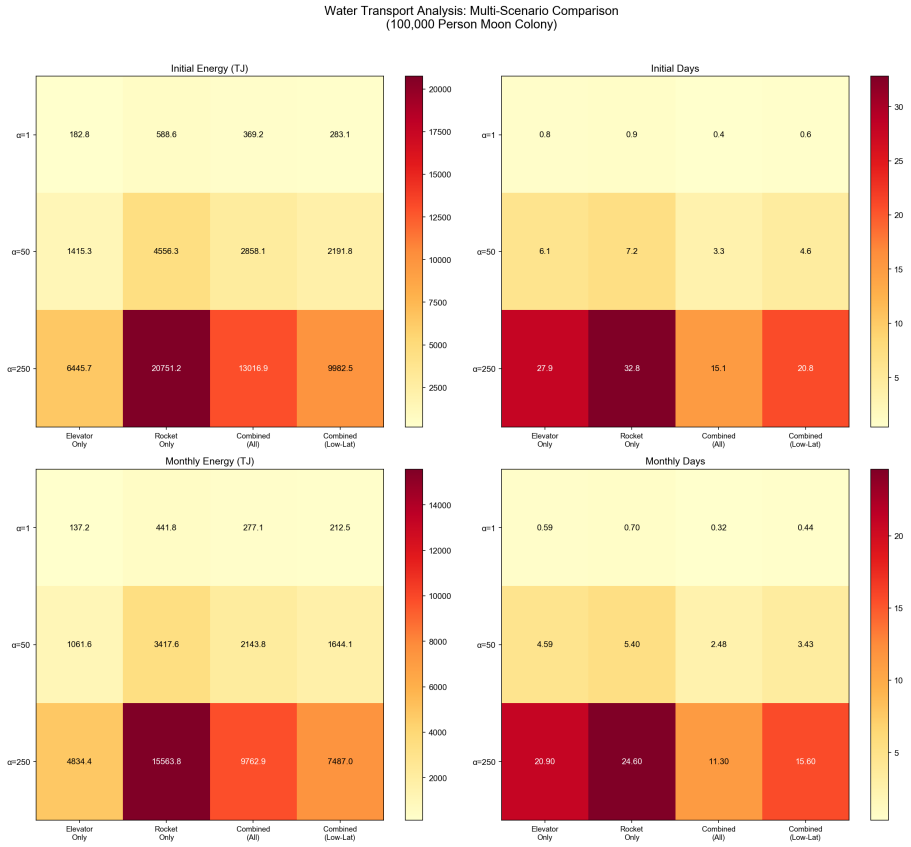

Figure 19: Heatmap of annual energy consumption across scenarios and transport schemes

The heatmap in Figure 19 reveals two critical trends:

- Energy consumption surges with α for all schemes.
- For any given α, Scheme 1 consistently exhibits the lowest energy footprint, confirming its superior efficiency.

3.5 Conclusion and Strategic Insights

1. **Trade-off between Comfort and Capacity**: Quantitative analysis confirms that quality of life acts as a logistical amplifier. At the Luxury tier, the annual water replenishment

occupies 69.68% of the theoretical annual capacity of the space elevator system. Maintaining high living standards significantly constricts the transport window for other critical infrastructure and scientific materials.

2. **Tiered Strategy Recommendations**:
    - **Initial Operations**: We recommend Survival tier combined with Scheme 1. This minimizes energy consumption while ensuring the survival threshold for 100,000 residents, reserving hybrid capacity for urgent infrastructure tasks.
    - **Mature Operations**: We recommend Comfort tier combined with Scheme 4. This provides a balance between speed and cost, completing the initial filling in 4.57 days with a reasonable energy footprint.
3. **System Resilience**: Thanks to the 90% efficient recycling system and the 30-day emergency buffer, the water logistics chain exhibits high resilience. Even during a full month of transport disruption, the survival of the colony remains uncompromised, allowing for logistical maintenance and error recovery.

4 Strengths and Weaknesses

4.1 Strengths

4.2 Weaknesses and Possible Improvement

5 Conclusion

References

[1] David R Francisco. “NASA-STD-3001 Volume 2, Revision E, NASA Spaceflight Human-System Standard Volume 2: Human Factors, Habitability, and Environmental Health”. In: *N/A* A (2025).

[2] Gunter’s Space Page. *Falcon-9*. https://space.skyrocket.de/doc_lau/falcon-9.htm. Accessed: 2026-02-01. Gunter’s Space Page, 2026.

[3] Hong Liu et al. “Review of research into bioregenerative life support system(s) which can support humans living in space”. In: *Life Sciences in Space Research* 31 (2021), pp. 113–120. ISSN: 2214-5524. DOI: https://doi.org/10.1016/j.lssr.2021.09.003. URL: https://www.sciencedirect.com/science/article/pii/S2214552421000663.

[4] Zephyr Penoyre and Emily Sandford. *The Spaceline: a practical space elevator alternative achievable with current technology*. 2019. arXiv: 1908.09339 [astro-ph.IM].

[5] Peter A Swan et al. “Space Elevators: An Assessment of the Technological Feasibility and the Way Forward”. In: *International Academy of Astronautics* (2013).

[6] Mihriban Whitmore, Jennifer Boyer, and Keith Holubec. “NASA-STD-3001, space flight human-system standard and the human integration design handbook”. In: *Industrial and systems engineering research conference*. JSC-CN-25695. 2012.

Report on Use of AI

1. OpenAI ChatGPT (Nov 5, 2023 version, ChatGPT-4,)

   Query1: <insert the exact wording you input into the AI tool>

   Output: <insert the complete output from the AI tool>

2. OpenAI Ernie (Nov 5, 2023 version, Ernie 4.0)

   Query1: <insert the exact wording of any subsequent input into the AI tool>

   Output: <insert the complete output from the second query>

3. Github CoPilot (Feb 3, 2024 version)

   Query1: <insert the exact wording you input into the AI tool>

   Output: <insert the complete output from the AI tool>

4. Google Bard (Feb 2, 2024 version)

   Query1: <insert the exact wording of your query>

   Output: <insert the complete output from the AI tool>